Anti-isostructural phases and anomalous thermoelasticity in In-based alloys: Synchrotron x-ray diffraction experiments and unified phenomenological model

V. P. Dmitriev,[1] D. Chernyshov,[1] Y. E. Filinchuk,[1] and V. F. Degtyareva[2]
[1]*Swiss-Norwegian Beam Lines at ESRF, Boîte Postale 220, 38043 Grenoble, France*
[2]*Institute of Solid State Physics, RAS, Chernogolovka, Moscow District, 142432 Russia*
(Received 20 September 2006; revised manuscript received 23 November 2006; published 17 January 2007)

A combined *in situ* high-temperature high-pressure synchrotron radiation diffraction study has been carried out on In alloys with Cd, Pb, and Sn. Anti-isostructural phase transitions between structures with opposite signs of tetragonal distortion, found earlier in In-Pb, have also been observed in In-Sn alloys. We show that negative thermal expansion of In and some of the In alloys is a phase-dependent effect resulting from a competition between spontaneous strain induced by a proper ferroelastic transformation and normal thermal expansion. A unified phenomenological model has been worked out for structural phase transitions in In and its alloys.

DOI: 10.1103/PhysRevB.75.024111 PACS number(s): 61.50.Ks, 61.66.Dk, 64.70.−p, 71.20.Be

I. INTRODUCTION

The anomalous elastic properties of the IIIA-group metal indium, and its crystal structure, unusual for metallic elements, give rise to intense studies, both experimental and theoretical. Elemental indium has at ambient conditions a body-centered tetragonal structure $[(c/a)_{fct}>1]$ with one atom in a primitive unit cell ($Z_p=1$) or, equally, two atoms in the Bravais cell. The close relation to the fcc structure makes it more convenient to use a face-centered tetragonal (fct) setting for body-centered tetragonal structures, which we do hereafter. A contraction (negative expansion) occurs in In along the fourfold axis and an expansion in the basal plane with increasing temperature.[1] One might have expected the tetragonal distortion to be removed by application of external pressure. However, high-pressure studies of In revealed the stability of the fct structure.[2,3] Moreover, it lowers the symmetry from tetragonal to orthorhombic at about 45 GPa.[4] By contrast, alloying In with the IIA-group metal Cd ($x_{Cd}>5$ at. %) on the IVA-group metal Pb ($x_{Pb}>30$ at. %) not only allows one to remove the tetragonal distortion of the crystal lattice and stabilize the face-centered cubic (fcc) structure,[5,6] but also switches the sign of the distortion and stabilizes another tetragonal structure (fct′) with $(c/a)_{fct}<1$ ($15<x_{Pb}<30$ at. %).

The rich and reliable experimental information accumulated for In-based alloys has stimulated, in the last decade, numerous theoretical works. Two approaches were developed in order to work out a unified model for In-based solid solutions. One, going back to an idea by Goodenough,[7] focused on the interaction between the Brillouin zone boundary planes and the Fermi surface (for a review, see Ref. 8 and references therein). The fitting of the Brillouin zone to the Fermi sphere provides, in the corresponding model, minimization of the electron band structure energy for the structures observed in In-based alloys. The other approach argues for an electron-controlled structural competition between the high-symmetry cubic and low-symmetry tetragonal structures. It was shown that the tetragonal distortion of the cubic structure leads to an increased hybridization of the 5*s* and 5*p* valence bands and, consequently, a gain of the band energy.[9–11] Despite the complexity of the problem, both approaches successfully accounted for some of the alloy properties; however, many aspects of their temperature and pressure behavior remain unclear so far. This is exemplified by In itself: no mechanism has been suggested explaining its negative thermal expansion, and no approach has been elaborated allowing understanding of the atypical behavior of the tetragonal distortion in the compressed metal.

There is one more unexplored aspect of the phase transitions occurring in In-based alloys—they are proper ferroelastic transformations. This is allows one, by applying a rather simple phenomenological formalism, to uncover the generic features of phase stability and crystal lattice transformations. This approach is symmetry based and, therefore, model-free. Its important advantage consists as well in easy incorporation of different external variables, like pressure, concentration, or temperature, so that, for instance, the latter is not restricted to $T=0$ K.

In this paper we show, using our recent as well as already published experimental data, that the temperature-pressure-concentration evolution of the crystal lattice of In-based alloys can be comprehensively accounted for in the framework of a unified phenomenological theory on a symmetry basis only. We show that the anomalous elastic effects in the alloys are of a nonequilibrium nature and they are induced by the same mechanism, which destabilizes the parent cubic structure.

II. EXPERIMENTAL METHODS

In situ high-temperature and high-pressure data were obtained at the Swiss-Norwegian beamline (BM1A) of the European Synchrotron Radiation Facility (ESRF, Grenoble, France). X-ray diffraction patterns were collected in angle-dispersive geometry using an image plate detector (MAR345). The monochromatic beam at wavelength $\lambda=0.7112$ or 0.7642 Å was slitted down to 70×70 μm^2. The sample-to-detector distance and the tilt angles of the detector were calibrated using Si and LaB_6 NIST standards. The two-dimensional diffraction images were analyzed using the ESRF FIT2D software,[12] yielding the one-dimensional intensity vs diffraction angle.

Small chips from polycrystalline alloy lumps were studied in an externally heated diamond-anvil cell (DAC) equipped

with diamonds beveled with 300 μm inner flat diameter. The samples were loaded into a hole of 120 μm in diameter drilled in stainless steel gaskets preindented to 30 μm thickness. Ruby provided the pressure calibration. Indium and In-rich alloys are soft enough to realize a quasihydrostatic environment in the gasket, which was controlled by a small broadening of the ruby fluorescence peaks. Nevertheless, in order to prevent a hypothetical reaction between the samples and the gasket material at nonambient conditions, silicone oil was used as pressure-transmitting medium. Diffraction measurements were performed up to a maximum pressure of 35 GPa.

The temperature effects at ambient pressure were studied with the samples filled into 300-μm-diameter glass capillaries ($400\times400\mu m^2$ slits) and heated with a hot air blower. The temperature calibration for the latter was performed by measuring the melting points of appropriate compounds and metals, including pure (99.999%) indium. The temperature dependence of the In lattice parameters then was used to calibrate, at ambient pressure, a *K*-type thermocouple placed inside the DAC. The temperature was stable within 1 K.

Rietveld refinement of the structures was performed using the FULLPROF package[13] with metal atoms at the 2*a* position with occupancies constrained to the nominal composition. The refined parameters were the scale factor, Debye-Waller factors, unit cell dimensions, and profile parameters. The typical error in lattice parameter determination was 10^{-4} Å; the error in the c/a ratio is estimated at 10^{-4}. The sample material was obtained by melting stoichiometric amounts of the pure elements (99.999% purity).

III. PHENOMENOLOGICAL THEORY

A. Model

It is convenient to classify a phase transition as ferroelastic if it involves a change in crystal system, accompanied by a change in strain owing to the difference in unit cell shape. Two subclasses, proper and improper, of ferroelastic transformations relate to those conserving the translation symmetry of the crystal, and breaking it with formation of a superstructure. The macroscopic spontaneous strain can be considered, therefore, as a symmetry-breaking order parameter for proper ferroelastic transformations but not for improper ones.

The experimentally measured strain $\varepsilon_1=(c_t/a_t-1)$ carrying the parent cubic lattice to a tetragonal one is one of two symmetry-equivalent strains:

$$\varepsilon_1=\frac{1}{\sqrt{6}}(e_1+e_2-2e_3),$$

$$\varepsilon_2=\frac{1}{\sqrt{2}}(-e_1+e_2) \tag{1}$$

which span the twofold irreducible representation E_g of the cubic point group O_h. The symmetrical combinations of the diagonal components e_i $(i=1-3)$ of the strain tensor can be, therefore, considered as order-parameter (OP) components for a cubic-to-tetragonal proper ferroelastic transformation. The group of two-dimensional matrices of the representation E_g (the so-called image group of the corresponding OP) is isomorphous to the vector representation of the point group C_{3v}. The corresponding nonequilibrium thermodynamic potential is a functional of two polynomials invariant by the cubic symmetry group of the parent phase:

$$I_1=\varepsilon_1^2+\varepsilon_2^2=\eta^2,$$

$$I_2=\varepsilon_1^3-3\varepsilon_1\varepsilon_2^2=\eta^3\cos3\varphi; \tag{2}$$

here $\tan\varphi=e_2/e_1$. The corresponding variational free energy (Landau potential) reads

$$F(P,T,\varepsilon_1,\varepsilon_2)\equiv\Phi(P,T,\eta,\varphi)=\Phi_0+a_1I_1+a_2I_2+a_{11}I_1^2+a_{12}I_1I_2+a_{111}I_1^3+a_{22}I_2^2. \tag{3}$$

The positive definiteness of the potential (3) yields the conditions $a_{111}>0$, and $a_{22}>0$. The model based on the order-parameter expansion (3) has been comprehensively discussed in Ref. 14 (see also Ref. 15 and references therein). The equations of state result from the minimization of Φ with respect to the variables η and φ (or F with respect to ε_1 and ε_2)

$$\frac{\partial\Phi}{\partial\eta}=2\eta(a_1+a_{11}I_1+3a_{111}I_1^2+a_{12}I_2)+3\eta^2\cos3\varphi(a_1+a_{12}I_1+2a_{22}I_2)=0, \tag{4}$$

$$\frac{\partial\Phi}{\partial\varphi}=-3\eta\sin3\varphi(a_2+a_{12}I_2+2a_{22}I_2)=0. \tag{5}$$

Equations (4) and (5) show that there are the following four possible equilibrium structures:

$$0:\quad \eta=0\quad \{\varepsilon_1=\varepsilon_2=0\},\quad Fm\bar{3}m(Z_P=1);$$

$$\text{I:}\quad \eta\neq0,\ \cos\varphi=1\quad \{\varepsilon_1=\varepsilon,\ \varepsilon_2=0;\ e_1=e_2>e_3\},\quad I4/mmm(Z_P=1);$$

$$\text{II:}\quad \eta\neq0,\ \cos\varphi=-1\quad \{\varepsilon_1=-\varepsilon,\ \varepsilon_2=0;\ e_1=e_2<e_3\},\quad I4/mmm(Z_P=1);$$

$$\text{III:}\quad (a_2+a_{12}I_2+2a_{22}I_2)=0\quad \{\varepsilon_1\neq0,\ \varepsilon_2\neq0;\ \varepsilon_1\neq\varepsilon_2\},\quad Fmmm(Z_P=1). \tag{6}$$

One can see that Eqs. (4) and (5) determine, in addition to the cubic parent phase 0, two low-symmetry phases I and II with identical tetragonal symmetry. They are associated with opposite values of the equilibrium order-parameter components, i.e., phases I and II are *anti-isostructural*.[15] The orthorhombic symmetry of phase III is the maximal common subgroup of the symmetry groups of phases I and II.

It follows from the theory of singularities that the model (3) is structurally stable.[16] The generic topology of the phase diagrams and anomalies predicted for the transition lines are invariant under small variations of the phenomenological pa-

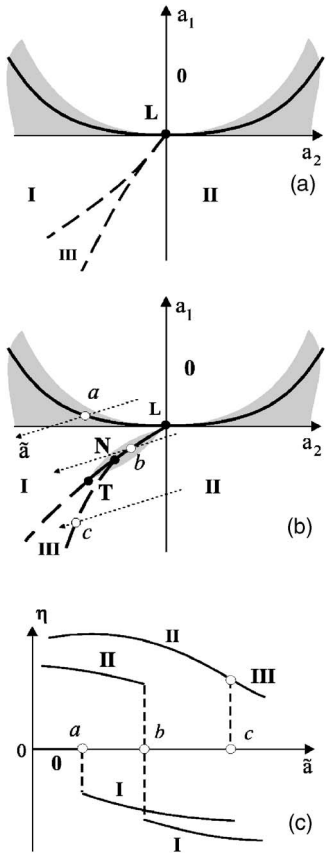

FIG. 1. (a), (b) Phase diagrams corresponding to the thermodynamic potential defined by Eq. (3) in the (a_1,a_2) plane. Diagrams are obtained for the following conditions: (a) $\Delta>0$, $a_{11}>0$; (b) $\Delta<0$, $a_{11}>0$. Solid lines are first-order transition lines. Dashed lines are second-order transition lines. Shadowed zones are the phase coexistence regions. L is the Landau point. T is a tricritical point, N is a triple point. Dotted lines denoted $a-c$ are the thermodynamic paths, that correspond to different sequences of phases. (c) Order-parameter variation for the various paths shown in (b).

rameters. The phase diagrams corresponding to the Landau potential (3) are displayed on Figs. 1(a) and 1(b). Their topology depends on (i) the sign of the phenomenological coefficients a_{12} and a_{11} in Eq. (3), which both remain unrestricted by the positive definiteness condition, as well as on (ii) the sign of the determinant

$$\Delta = \begin{vmatrix} \frac{\partial^2\Phi}{\partial I_1^2} & \frac{\partial^2\Phi}{\partial I_1 \partial I_2} \\ \frac{\partial^2\Phi}{\partial I_1 \partial I_2} & \frac{\partial^2\Phi}{\partial I_2^2} \end{vmatrix} = 4a_{11}a_{22} - a_{12}^2. \quad (7)$$

The case of $\Delta<0$ [Fig. 1(b)] is of special interest for our consideration. A negative value of Δ partly suppresses the stability domain of the orthorhombic phase III in the vicinity of the Landau point L ($a_1=0$, $a_2=0$), and leads to a direct first-order anti-isostructural transition between phases I and II. The space groups of these two phases are the same but the sign of the order-parameter components changes from one phase to another [Fig. 1(c)]. In terms of the spontaneous strain tensor components one has in one phase $e_3>e_2=e_1$, whereas in the other phase $e_3<e_2=e_1$ [see Eqs. (6)]. Accordingly, in the case of a cubic-to-tetragonal transformation, two anti-isostructural phases are associated with the opposite signs of the tetragonal distortion $(c/a-1)$. It has already been stressed in the pioneering papers by Landau[17] that the point L ending a line of first-order transitions, which separates two anti-isostructural phases, is an isolated point of a second-order phase transition.

The order parameter is determined as a function of phenomenological coefficients from the potential (3) by Eqs. (4) and (5). In the parent phase 0 it has an a_i-independent value $\eta=0$, whereas in the distorted phases I, II, and III η varies with a_i as expressed by the equations of state. Figure 1(c) shows the shape of $\eta(\tilde{a})$ along thermodynamic paths defined by straight lines $\tilde{a}=\alpha_0 a_1+\beta_0 a_2$ in the (a_1,a_2) plane, which correspond to various sequences of the phases as indicated in Fig. 1(b).

B. Application to In-Pb system

The overall phenomenological Landau approach, developed in Sec. III A can be tested against available structure data obtained at room temperature as a function of pressure, across the In-Pb system. Pure indium metal crystallizes in a body-centered tetragonal structure ($I4/mmm$, $Z_P=1$),[6] which corresponds to a slightly distorted face-centered cubic structure with $(c/a)_{fct}=1.076$ [phase II in Eq. (6)]. High-pressure x-ray diffraction experiments revealed that the c/a ratio increases with pressure, reaching a maximum around 24 GPa, and then unusually decreases with further compression.[2] At 45 GPa indium transforms to a face-centered orthorhombic (fco) phase $Fmmm$ ($Z_P=1$),[4] which is obtained by a simple orthorhombic distortion of the low-pressure tetragonal phase.[18] One notices that this sequence corresponds to the path c in Fig. 1(b). The $In_{0.90}Pb_{0.10}$ alloy has at ambient conditions the In-type fct structure with $c/a>1$ (phase II). Under pressure, it undergoes a phase transition to another tetragonal structure, with a discontinuous jump of the axial ratio from $c/a>1$ (phase II) to $c/a<1$ (phase I),[19] i.e., it follows the path b in Fig. 1(b).

The Pb-enriched alloys $In_{.85}Pb_{.15}$ and $In_{.78}Pb_{.22}$ crystallize in the fct′ structure (phase I) and show no phase transition up to, at least, 40 GPa.[20] $In_{1-x}Pb_x$ alloys with $30>x>60$ at. % have a cubic structure [parent phase 0 in Eq. (6)] and transform under pressure from the fcc to fct′ structure with $c/a<1$ (phase I),[21] which corresponds to the path a.

Therefore, all the above features of the phase evolution in In-Pb alloys are evidently accounted for in the framework of the phenomenological model with the Landau potential (3).

Figure 2 shows a phase diagram identical to Fig. 1(b) but complemented with an order parameter η as the third dimension. Equations of state (4) and (5) yield equations for the surfaces corresponding to different phases in Fig. 2. The condition $\eta(a_1,a_2)=0$ naturally defines the plane of the parent phase 0 while the equations

$$2a_1 \pm 3a_2\eta + 4a_{11}\eta^2 \pm 5a_{12}\eta^3 + 6(a_{111}+a_{12})\eta^4 = 0 \quad (8)$$

correspond to the phase sheets I (positive odd-degree terms) and II (negative odd-degree terms). It is convenient, in the

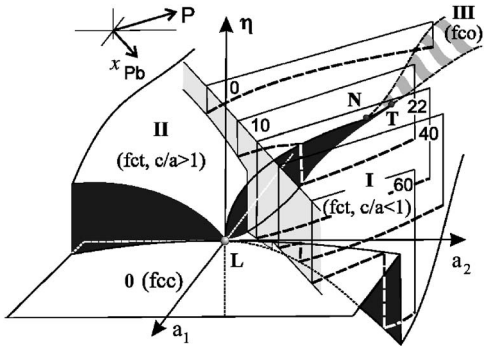

FIG. 2. Equilibrium phase diagram corresponding to the thermodynamic potential (3), in the (a_1, a_2, η) space, obtained for the conditions $\Delta<0$, $a_{11}>0$. Grayish plane is an ambient isobaric plane. Vertical planes are the (η, P) isothermal sections, which correspond to $In_{1-x}Pb_x$ with different Pb content. Dashed lines in the planes show the order parameter $\eta=(c/a-1)$ as a function of pressure. The numbers indicate the atomic percentage of lead. Special points are the same as in Fig. 1.

Landau theory, to consider only phenomenological coefficients in the lowest-degree terms to be linearly dependent on external thermodynamic parameters temperature T, pressure P, and concentration x:

$$a_1 = \alpha_1(T - T_C) + \beta_1(P - P_C) + \gamma_1(x - x_C),$$

$$a_2 = \alpha_2(T - T_C) + \beta_2(P - P_C) + \gamma_2(x - x_C). \qquad (9)$$

Such an assumption seems to be valid for the In-Pb alloys. Indeed, one finds that the plane sections of the theoretical diagram [Fig. 1(c) and Fig. 2] perfectly reproduce the evolution of the order parameter $\eta=(c/a-1)$ as a function of pressure experimentally obtained by different authors.[2–4,19–21] In particular, the phenomenological model predicts the existence of a maximum on the $\eta(p)$ curve for pure indium metal, which foregoes the continuous transformation to an orthorhombic phase [Fig. 1(c)].

The correct mapping of the structural phases and pressure dependence of $\eta=(c/a-1)$ implies that the symmetry-based theory with the nonequilibrium potential (3), along with the phenomenological hypothesis (9), gives a unifying picture of the phase stability and pressure-controlled elastic behavior for $In_{1-x}Pb_x$ alloys. This conclusion encouraged us to study pressure- and temperature-induced elastic strains in other In-based alloys, namely, $In_{1-x}Sn_x$ and $In_{1-x}Cd_x$, in order to validate the phenomenological model.

IV. RESULTS AND DISCUSSIONS

A. In-Sn system

Alloying In with Pb or Sn metal leads to an increase of the valence p-electron concentration. The similarity in the effect of the two additives results in an analogy in structure sequences for the In-Pb and In-Sn systems: at ambient conditions $In_{1-x}Sn_x$ alloys with $x<10$ at. % have the In-type tetragonal structure with $c/a>1$ (phase II); with $13<x<25$ at. % the alloys stabilize in a tetragonal structure with

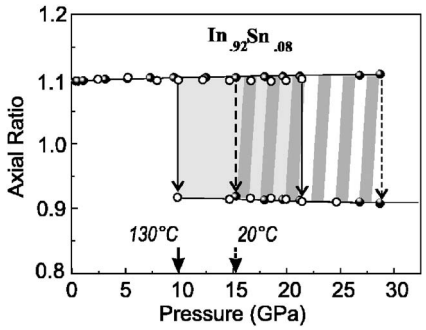

FIG. 3. Pressure variation of the axial ratio c/a for In alloy with 8 at. % Sn at room temperature (solid dots) and 130 °C (open dots). Error bars are smaller than symbol size. Gray and hatched areas indicate the corresponding two-phase regions.

$c/a<1$ (phase I).[5] It should be noted, however, that the analogy with the In-Pb alloying process, as well as the validity of the phenomenological theory, are restricted for $In_{1-x}Sn_x$ to $x<25$ at. % as at higher Sn concentration the alloys adopt a simple hexagonal structure.[5] A previous high-pressure study[22] of $In_{0.80}Sn_{0.20}$ confirms its similarity to the corresponding Pb-containing alloy. Phase I was found to be stable up to 30 GPa, the highest pressure reached in the experiment, whereas the degree of tetragonal distortion increases in full agreement with the predictions of the phenomenological model. Our present work shows identical pressure behavior also for Sn- and Pb-containing indium alloys with lower concentration of the group-IVA elements.

The $In_{0.82}Sn_{0.08}$ alloy, at ambient pressure and temperature, has a fct (phase II) structure with $c/a=1.096$ ($a=4.6145$ Å, $c=5.0571$ Å). It remains stable up to $\approx$15 GPa but transforms at higher pressure, through an extended two-phase region, to the phase I with the same tetragonal structure but with $c/a<1$ (Fig. 3). Thus, similarly to $In_{1-x}Pb_x$ ($x\leqslant 10$), the $In_{0.82}Sn_{0.08}$ alloy undergoes under pressure an anti-isostructural phase transition from one tetragonal phase to another with a discontinuous drop of the axial ratio from $c/a=1.104$ to $c/a=0.92$ ($a=4.3414$ Å, $c=4.7928$ Å; $a'=4.5664$ Å, $c'=4.20$ Å at 15 GPa). The pressure range of the two-phase mixture is about 13 GPa.

We have found that the temperature increase does not change, at least within the accuracy of our experiment, the character of the antiisostructural fct-to-fct′ phase transition. Compression of $In_{0.82}Sn_{0.08}$ at $T=130$ °C (the melting point for this alloy is about 150 °C) results in the same axial ratio discontinuity (Fig. 3) but shifts the transformation point to a lower pressure of 9.9 GPa ($a=4.4258$ Å, $c=4.8665$ Å; $a=4.7093$ Å, $c=4.4257$ Å). The transformation process remains sluggish over the two-phase coexistence pressure range of about 11 GPa similar to that at room temperature.

By mapping the data onto a phase diagram, one concludes that there is a negative slope of the I-II phase boundary on the P-T plane. On the theoretical phase diagram the temperature axis proves, therefore, to be nearly parallel to the a_1 axis but opposite in direction to the P axis. Figure 4 summarizes the experimental data on the In-Sn system in the form of the theoretical phase diagram, similarly to Fig. 2 for the In-Pb system.

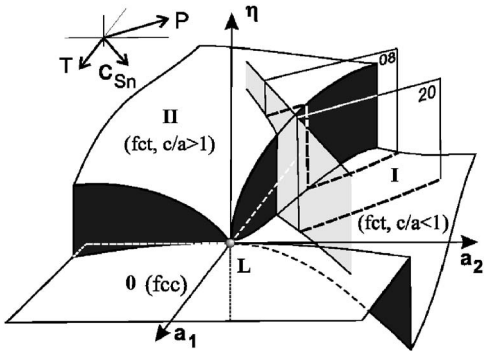

FIG. 4. Isothermal-isoconcentration sections of the theoretical phase diagram for $In_{1-x}Sn_x$. Notations are the same as on Fig. 2.

Thus the phase transition phenomena in In-Sn alloys, like their Pb analogs, can be successfully parametrized by the phenomenological model (3). However, the practical limits of the model extend only to $x_{Sn} < 25$ at. %.

B. In-Cd alloy

In contrast to the IVA metals Pb and Sn, alloying In with the group-IIA metal Cd leads to a decrease of the valence *p*-electron concentration. Alloying with 5 at. % of Cd results in a discontinuous change of the structure from fct (phase II) to fcc (phase 0). $In_{0.94}Cd_{0.06}$ transforms, at 1.4 GPa, from the parent cubic structure into the fct (phase II) structure.[21] The latter phase is stable up to at least 30 GPa. In order to place the In-Cd alloy onto the general phase diagram we studied two compounds $In_{0.96}Cd_{0.04}$ and $In_{0.94}Cd_{0.06}$ with the Cd content close to the critical.

Figure 5 shows the evolution of the diffraction patterns for $In_{0.96}Cd_{0.04}$ during a heating-cooling cycle. The alloy sample transforms, at around $T=80$ °C, from the fct ($a=4.6780$ Å, $c=4.7617$ Å, $c/a=1.018$ at $T=77$ °C) to the

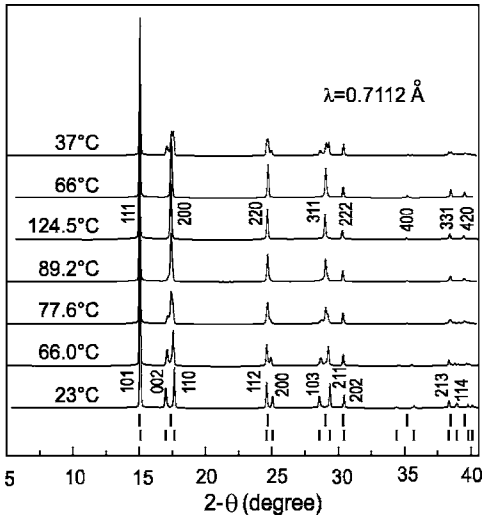

FIG. 5. Selected x-ray diffraction patterns of $In_{0.96}Cd_{0.04}$ at different temperatures, at ambient pressure. The tick marks indicate the positions of calculated Bragg reflections for fcc (upper set) and fct (lower set) structures.

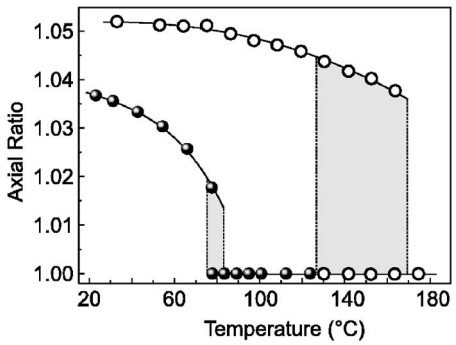

FIG. 6. Temperature dependence of the axial ratio c/a for $In_{0.96}Cd_{0.04}$ at ambient pressure (solid dots) and $In_{0.94}Cd_{0.06}$ at 5 GPa (open circles). Error bars are smaller than symbol size. Two-phase coexistence regions are shaded.

fcc structure ($a=4.7041$ Å at $T=83$ °C) displaying a small discontinuity in the c/a axial ratio (Fig. 6) over a short (~10 °C) phase coexistence range. The transformation is reversible and accompanied by a remarkable temperature hysteresis (at least 50 °C; see Fig. 5) indicative of a first-order transformation.

Another alloy, $In_{0.94}Cd_{0.06}$ with the fcc structure at ambient conditions, was treated in two different regimes: (i) isothermal compression at room temperature, and (ii) isobaric heating at elevated pressure.

(i) During the first calibration experiment fcc $In_{.94}Cd_{.06}$ transformed, at $P=1.5$ GPa, to the fct structure (phase II) with a c/a ratio jump of ~0.0375 (Fig. 7) This is in full agreement with results of a previous study.[21] The fct phase remains stable up to 35 GPa.

(ii) The second cycle started with compressing the sample to 5 GPa (double dot in Fig. 7) where only the fct phase is stable, and then was followed by quasi-isobaric heating. Figure 8 shows selected diffraction patterns collected at different stages of the sample treatment. The sample transforms on heating from fct ($a=4.5198$ Å, $c=4.7313$ Å at $T=120$ °C) back to fcc ($a=4.5896$ Å at $T=130$ °C) phase reversibly and discontinuously at $T \simeq 127$ °C. The progressive decrease of the tetragonal distortion as a function of temperature is similar to that at pressure release (Figs. 6 and 7). The magnitude of the temperature-induced jump in the c/a ratio is very

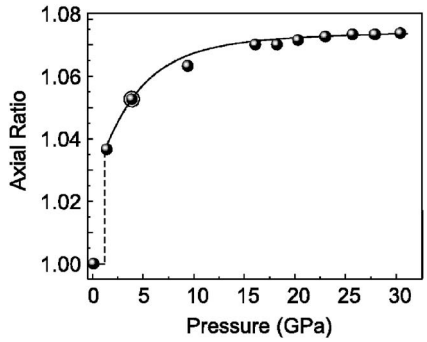

FIG. 7. Variation of the axial ratio c/a for $In_{0.94}Cd_{0.06}$ alloy as a function of pressure, at room temperature. Error bars are smaller than symbol size. The solid line is a guide for the eye.

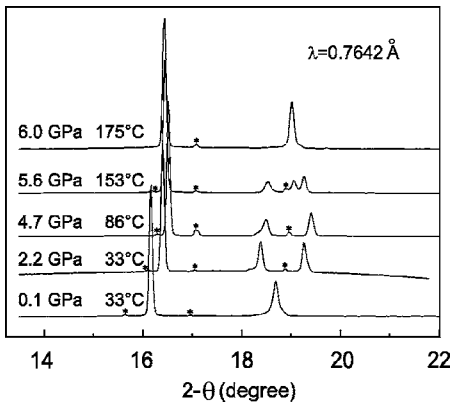

FIG. 8. Selected diffraction patterns collected during pressure-temperature treatment of the $In_{0.94}Cd_{0.06}$ sample. Asterisks mark peaks from a small admixture of the hexagonal Cd.

close to the pressure-induced one (Fig. 7) but exceeds significantly the discontinuity observed at the fct-fcc transformation in $In_{0.96}Cd_{0.04}$ (compare the curves in Fig. 6).

Figure 9 summarizes the data obtained for the Cd-containing alloys. The occurrence of the II-0 phase transition at both compositions, as well as an apparent increase of the order-parameter jump with increasing Cd concentration, unambiguously define the direction for the P, T, and x axes on the (a_1, a_2) plane. Similar to all systems discussed above, pressure and temperature appear in the In-Cd system to be counteractive factors.

Therefore, also for the In-Cd system, the phase transitions and structural deformations as a function of concentration, pressure, and temperature are in agreement with the phenomenological model (3). The concentration of Cd, x_{Cd}, has an opposite effect on the phase stability to the concentration of Pb and Sn, $x_{Pb/Sn}$. This can be correlated with an increase (for Pb and Sn) and decrease (for Cd) of the p-electron concentration.

C. Thermal expansion of the alloys at ambient pressure

An important question, which this paper addresses, regards the origin of the remarkable thermoelastic anisotropy

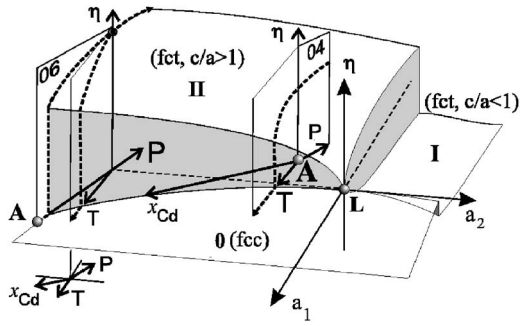

FIG. 9. Equilibrium phase diagram corresponding to the thermodynamic potential (3), in the (a_1, a_2, η) space, worked out at $\Delta < 0$, $a_{11} > 0$. Vertical planes, denoted by the concentration x, are isobaric and isothermal sections for the two $In_{1-x}Cd_x$ alloys ($x=4$ and 6 at. %). L is the Landau point. Points A show the states of the two alloys at ambient conditions. Dotted lines correspond to the experimentally observed dependences $\eta(P)$ and $\eta(T)$.

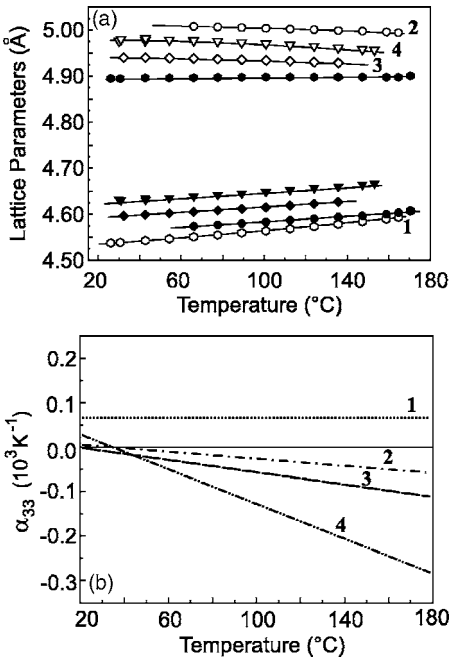

FIG. 10. (a) Thermal expansion of In-based alloys. Circles correspond to $In_{0.92}Sn_{0.08}$, triangles $In_{0.90}Pb_{0.10}$, diamonds In, and hexagons $In_{0.78}Pb_{0.22}$. Open spots correspond to the lattice parameter c, closed to a. Error bars are smaller than symbol size. Solid lines serve as guides for the eye. (b) Temperature variation of the principal expansion coefficient α_{33} for $In_{0.78}Pb_{0.22}$ (1), $In_{0.92}Sn_{0.08}$ (2), In (3), and $In_{0.90}Pb_{0.10}$ (4). Related curves in (a) and (b) are marked with identical numbers.

in pure In metal and In-based alloys. The thermal expansion coefficient α_{11} perpendicular to the tetragonal axis is positive, but the coefficient α_{33} parallel to the axis is negative and decreases with increasing temperature.[1] However, accurate measurements on pure In samples and its alloys with Pb, Sn, and Cd allow us to conclude that the above feature is characteristic of the tetragonal structure with $c/a > 1$, i.e., of phase II, but not of phase I with $c/a < 1$ (Fig. 10). The sign of α_{33} correlates, therefore, with the sign of the ferroelastic OP.

Simultaneous heating of fct and fct′ phases in identical conditions provides us with clear evidence that pressure and concentration play only a secondary role in the effect. We have managed to obtain a fct-fct′ two-phase mixture for one of the In-Pb alloys at ambient conditions. Following Fig. 2, an alloy with near critical concentration $x_{Pb}=10$ at. % is very close at ambient conditions to the fct-fct′ transition line, so that the difference in energy between a stable phase II and a metastable phase I should be very small and the corresponding energy barrier should be tiny. The latter particular features of the In energy landscape has already been demonstrated by first-principles calculations.[10,11] We found that the phase content of $In_{0.90}Pb_{0.10}$ samples depends on the preparation procedure. The original alloy lumps are single phase with only the phase II present. Although small chips cut with a blade remain single phase, rasping the lump transforms a part of the sample powder to phase I. Figure 11 shows the experimental diffraction pattern from the rasped $In_{0.90}Pb_{0.10}$ alloy and the best fit with two tetragonal structures, fct′

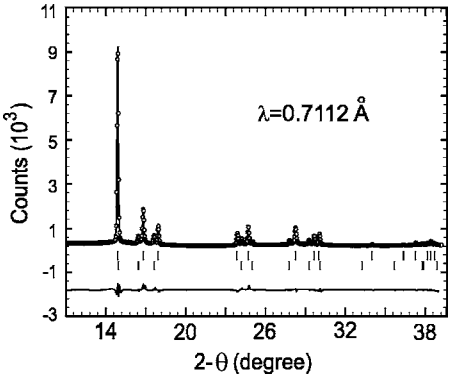

FIG. 11. Diffraction pattern and the respective Rietveld fit of the fct/fct two-phase mixture in $In_{0.90}Pb_{0.10}$ at ambient pressure. Circles represent experimental data; the solid line running through data refers to the calculated pattern. The corresponding difference curve is plotted below. The tick marks indicate positions of Bragg peaks for the fct (top) and the fct′ (bottom) structures.

(phase content 85 vol %) and fct (15 vol %). The corresponding unit cell lattice parameters are $a=4.8613$ Å, $c=4.5415$ Å; $a=4.6284$ Å, $c=4.9821$ Å; the reliability indices $R'_B=7.72\%$, $R'_F=6.92\%$; $R_B=7.14\%$, $R_F=5.67\%$. Shear stresses induced by rasping induce, therefore, a transition between fct and fct′ structures even at ambient conditions. The fct′ (I) structure is retained in the sample up to $T=135$ °C (melting point for the alloy is $T=150$ °C), and then irreversibly transforms to fct (II).

Although heated now in identical conditions, the fct (phase II) and the fct′ (phase I) structures exhibit, nevertheless, different thermoelastic behavior. The stable fct structure contracts along the fourfold axis with increasing temperature, while the metastable fct′ one expands in this direction (Fig. 12).

Let us show that the above effects can also be accounted for in the framework of the unified phenomenological model as suggested above for the In-based alloys. The total strain induced in a distorted structure by a temperature variation consists of two parts:

$$\varepsilon_T = \varepsilon_{th} + \varepsilon_{OP}, \tag{10}$$

where ε_{th} corresponds to ordinary thermal expansion (nonsymmetry breaking), and ε_{OP} is the spontaneous strain induced by a ferroelastic phase transition (symmetry breaking). The thermal expansion of a tetragonal structure is entirely characterized by the two principal linear expansion coefficients $\alpha_1=\alpha_{11}=\alpha_{22}=(\partial\varepsilon_1/\partial T)=(\partial a/\partial T)/a$, and $\alpha_3=\alpha_{33}=(\partial\varepsilon_3/\partial T)=(\partial c/\partial T)/c$. Since the tetragonal structure can be considered as a distorted cubic structure, as in the case of In alloys, the latter coefficient takes the form $\alpha_3=\alpha_1^c+\alpha_{cr}$, where α_1^c is the coefficient for the cubic structure, and $\alpha_{cr}=1/c\partial(\Delta c)/\partial T\cong\partial\eta/\partial T$ is the "critical" (symmetry-breaking) contribution of an order parameter reducing symmetry from cubic to tetragonal. The order-parameter values for phases I and II should be found as solutions of the equations of state (8). Our analysis of experimental data on the In-based alloys concludes that the consideration can be restricted, without loss of generality, to the vicinity of the Landau point (see Figs. 2, 4, and 9) where fourth-degree terms dominate over the sixth-degree one. It allows us, in turn, to restrict the Landau expansion (3) to the fourth degree terms. A simplified quadratic equation yields two solutions:

$$\eta_{I,II} = \frac{\mp 3a_2 \pm (9a_2^2 + 32a_1a_{11})^{1/2}}{8a_{11}}. \tag{11}$$

One of them corresponds to phase I (upper signs in the numerator) and the other to phase II (lower signs).

Since the direction of the T axis is parallel to the axis a_1, all other phenomenological coefficients are temperature independent [$\alpha_1 a>0$, $\alpha_2\approx 0$ in Eq. (9)]. This yields

$$\alpha_{cr}^{I,II} \simeq \left(\frac{\partial\eta}{\partial T}\right)_{P,x} = \pm 2\alpha_1[9a_2^2 + 32\alpha_1(T-T_C)a_{11}]^{1/2}. \tag{12}$$

The extra term in the equilibrium cubic expansion coefficient is positive in phase I (upper sign), and negative in phase II (lower sign). The latter decreases when the temperature rises approaching T_C: $\alpha_{cr}\propto -(T-T_C)^{-1/2}$. Thus, α_3 may become negative, and it should decrease. Figure 9, as well as Figs. 2 and 4, clearly shows how the order parameter $\eta=(c_t/a_t-1)$ decreases in phase II with a temperature increase, i.e., how the lattice parameter c_t decreases on approaching a_t. As this negative contribution becomes dominant, it results in uniaxial contraction (negative expansion) of the tetragonal lattice.

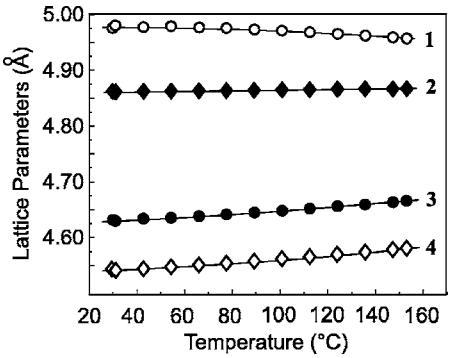

FIG. 12. Temperature variation of the lattice parameters for $In_{0.90}Pb_{0.10}$ in phases I and II, at ambient pressure: (1) c_{II}, (2) a_I, (3) c_I, and (4) a_{II}. Error bars are smaller than symbol size.

V. CONCLUSIONS AND OVERLOOK

A unified phenomenological theory has been worked out for In-based alloys. It maps all the structural phases experimentally observed so far, and correctly describes transitions between them. The model discloses the origin of the anomalous elastic anisotropy as being related to the spontaneous strain induced by a proper ferroelastic transition. When looking for a microscopic mechanism for the macroscopic elastic instability one should rely on the symmetry of the order parameter as a selection criterion. On one hand, it is convenient to consider the structural effects in In metal and its alloys as electron driven. On the other hand, our analysis assigns the

ferroelastic order parameter to the center of the Brillouin zone (BZ) and attributes it to the twofold irreducible representation E_g of a cubic group. Thus, the proper functions of the mechanism have to transform as symmetrical combinations of diagonal components of a second-rank tensor (see Sec. III A). These symmetry considerations point to the $4d$ core electrons as those having proper symmetry and therefore potentially related to the primary (symmetry-breaking) factor of the structural stability. It should be noted that an important broadening of the $4d$ core band and its strong overlap with the $5s$ band at the BZ center under high pressure have already been disclosed in In under high pressure by first-principles calculations.[9] More sophisticated than a simple *sd* type, an sp^2 hybridization also satisfies the symmetry conditions. Some other electron effects, including those at the BZ boundary, may play a significant but secondary (non-symmetry breaking) role in the structure evolution scenario.

Alloying In with IIA- and IVA-group metals provides an extraordinary example of proper ferroelastic compounds. To the best of our knowledge, this is the first case when variation of external thermodynamical parameters (T,P,x) reveals the complete variety of stable phases and phase transitions between them, predicted by a theory with a multicomponent order parameter. This theory is applied in particular to direct transitions between anti-isostructural phases. Only the Landau point is still missing on the experimental diagrams of the alloys. We failed to tune the variables P, T, and x in order to pass through it. However, earlier publications on the study of nanosized samples of pure[23] In and In-Pb alloys[24] suggest the way to fill this gap. It has been found that the phase stability is size dependent, and In crystallites of 5 nm in diameter and $In_{0.89}Pb_{0.11}$ ones of 10 nm in diameter possess a fcc structure at ambient conditions. This means that the plane $P=0$ in Fig. 2 is shifted so that the "active field" includes also the Landau point so that it becomes experimentally accessible.

[1] V. T. Deshpande and R. R. Pawar, Acta Crystallogr., Sect. A: Cryst. Phys., Diffr., Theor. Gen. Crystallogr. **25**, 415 (1969).
[2] K. Takemura, Phys. Rev. B **44**, 545 (1991).
[3] O. Schulte and W. B. Holzapfel, Phys. Rev. B **48**, 767 (1993).
[4] K. Takemura and H. Fujihisa, Phys. Rev. B **47**, 8465 (1993).
[5] *A Handbook of Lattice Spacings and Structures of Metals and Alloys*, edited by W. B. Pearson (Pergamon, Oxford, 1964), Vols. 1 and 2.
[6] P. Villars and L. D. Calvert, *Pearson's Handbook of Crystallographic Data for Intermetallic Phases* (American Society for Metals, Metals Park, OH, 1985).
[7] J. B. Goodenough, Phys. Rev. **89**, 282 (1953).
[8] V. F. Degtyareva, Phys. Usp. **49**, 369 (2006).
[9] S. I. Simak, U. Häussermann, R. Ahuja, S. Lidin, and B. Johansson, Phys. Rev. Lett. **85**, 142 (2000).
[10] A. S. Mikhaylushkin, U. Häussermann, B. Johansson, and S. I. Simak, Phys. Rev. Lett. **92**, 195501 (2004).
[11] A. S. Mikhaylushkin, S. I. Simak, B. Johansson, and U. Häussermann, Phys. Rev. B **72**, 134202 (2005).
[12] A. P. Hammersley, S. O. Svensson, M. Hanfland, A. N. Fitch, and D. Hausermann, High Press. Res. **14**, 235 (1996).
[13] J. Rodriguez-Carvajal, Physica B **192**, 55 (1993).
[14] Yu. Gufan, *Structural Phase Transitions* (Nauka, Moscow, 1982) (in Russian).
[15] P. Toledano and V. Dmitriev, *Reconstructive Phase Transitions in Crystals and Quasicrystals* (World Scientific, Singapore, 1996).
[16] E. I. Kut'in, V. L. Lorman, and S. V. Pavlov, Sov. Phys. Usp. **36**, 497 (1991).
[17] L. D. Landau, Zh. Eksp. Teor. Fiz. **7**, 19 (1937); **7**, 627 (1937); translated in *Collected Papers of L. D. Landau,* edited by D. Ter Haar (Pergamon Press, Oxford, 1965), pp. 193 and 216.
[18] This transition was not observed in the experiments by Schulte and Holzapfel (Ref. 3). However, taking into account the continuous character of the fct-to-fco (II-to-III in Fig. 1) transformation and, consequently, small peak splittings, the inconsistency might be due to the lower resolution of the energy-dispersive technique employed in Ref. 3.
[19] V. F. Degtyareva, I. K. Bdikin, F. Porsch, and N. I. Novokhatskaya, J. Phys.: Condens. Matter **15**, 1635 (2003).
[20] V. F. Degtyareva, I. K. Bdikin, F. Porsch, and N. I. Novokhatskaya, High Press. Res. **24**, 551 (2004).
[21] O. Degtyareva, V. F. Degtyareva, F. Porsch, and W. B. Holzapfel, J. Phys.: Condens. Matter **13**, 7295 (2001).
[22] O. Degtyareva, V. F. Degtyareva, F. Porsch, and W. B. Holzapfel, J. Phys.: Condens. Matter **14**, 389 (2002).
[23] A. Yokozeki and G. D. Stein, J. Appl. Phys. **49**, 2224 (1978).
[24] K. Asaka, E. Kitahata, Y. Hirotsu, K. Kifune, Y. Kubota, and T. Tadaki, Scr. Mater. **44**, 2043 (2001).